

Wetting transparency of graphene

Javad Rafiee^{1†}, Xi Mi^{2†}, Hemtej Gullapalli³, Abhay V. Thomas¹, Fazel Yavari¹, Yunfeng Shi², Pulickel M. Ajayan^{3*} and Nikhil A. Koratkar^{1,2*}

We report that graphene coatings do not significantly disrupt the intrinsic wetting behaviour of surfaces for which surface-water interactions are dominated by van der Waals forces. Our contact angle measurements indicate that a graphene monolayer is wetting-transparent to copper, gold or silicon, but not glass, for which the wettability is dominated by short-range chemical bonding. With increasing number of graphene layers, the contact angle of water on copper gradually transitions towards the bulk graphite value, which is reached for ~6 graphene layers. Molecular dynamics simulations and theoretical predictions confirm our measurements and indicate that graphene's wetting transparency is related to its extreme thinness. We also show a 30–40% increase in condensation heat transfer on copper, as a result of the ability of the graphene coating to suppress copper oxidation without disrupting the intrinsic wettability of the surface. Such an ability to independently tune the properties of surfaces without disrupting their wetting response could have important implications in the design of conducting, conformal and impermeable surface coatings.

Graphene is a single-atom-thick sheet of sp^2 -hybridized carbon atoms arranged in a hexagonal honeycomb lattice. It possesses a unique combination^{1,2} of high specific surface area, chemical stability, mechanical strength, flexibility, high electrical and thermal conductivity, tunable bandgap, as well as being optically transparent. The optical absorption of a single graphene layer is shown to be ~2.3% over the visible spectrum^{3–5}, which combined with its high electrical conductivity^{6–8} could lead to transparent conductive electrodes^{9–11}. In spite of intense activity in graphene research, there are very few reports studying water–graphene interactions^{12–14}, which could be important if graphene is to be used in conformal coatings. Motivated by this, we performed water contact-angle measurements on graphene sheets deposited on a variety of substrates. On surfaces such as copper, gold or silicon, where van der Waals forces control the wetting, we find that graphene remains transparent to the substrate wetting behaviour and remains non-invasive to the substrate/water interface. We call this effect the wetting transparency of graphene. To our knowledge this is the first report of such wetting transparency and could open the door to a variety of applications. In particular, hydrophobic and super-hydrophobic surfaces have low surface energy and are generally electrically insulating. Conformal coating of graphene on such surfaces could result in a new class of conductive super-hydrophobic surfaces with possible uses in a variety of applications^{15–18}.

Large-area monolayer graphene films were synthesized by chemical vapour deposition (CVD) on Cu foils using the liquid precursor hexane¹⁹. After growth, a thin poly(methylmethacrylate) (PMMA) film was coated on the graphene/Cu substrate. The underlying Cu substrate was dissolved in dilute HNO_3 , and the

film was transferred onto both Si and Au substrates. Films with a varying number of graphene layers (N), from monolayer to $N > 10$, were also deposited on Cu and glass substrates. Control of the number of layers was carried out by varying the growth time in CVD, as demonstrated in our previous work¹⁹. Atomic force microscopy was used to measure the film thickness, which gave estimates of the number of graphene layers in each sample. Graphene-coated Cu and glass samples with N values ranging from 1, 1–2, 2–3, 4–6, 6–9, 8–12 and 10–15 were prepared. Figure 1a–c shows optical micrographs of large-area graphene film deposition on Cu, glass and Si, respectively. The deposited graphene is several cm in in-plane dimensions and forms a uniform conformal coating with no physical breaks. A Raman spectroscopy study (using 514 nm wavelength excitation) was used to confirm the approximate number of graphene layers on the Cu substrates. Figure 1d shows measured Raman spectra for the 2D peak for graphene films with a varying number of layers. A clear shift in the position of the 2D peak with number of layers is observed (Fig. 1d,e), from ~2,680 cm^{-1} for monolayer graphene to ~2,715 cm^{-1} for the $N > 10$ sample. These results are consistent with the literature; for example, Ferrari *et al.*²⁰ have reported that, as the number of layers in graphene films is reduced, the 2D peak shifts towards a lower frequency range, and for single-layer graphene it appears between 2,650 and 2,700 cm^{-1} .

Static water contact-angle measurements were performed by placing droplets of de-ionized water on the various graphene-coated substrates (see Methods). For statistics, 6–10 separate measurements were performed at different locations on the sample surface and the results were averaged to obtain the mean and standard deviation. The precautions taken to clean and prevent oxide layer formation on the substrates, and to remove residual PMMA from the graphene surfaces before performing the wetting experiments, are described in the Methods. Figure 2a shows the measured results for the water contact angle on Si and on a ~300 nm thick Au film on Si, with and without a monolayer graphene coating. The baseline (uncoated) Si and Au contact angles are ~32.6° and ~77.4°, respectively. A monolayer graphene coating results in only a ~1–2% increase in the contact angles of Si and Au. The wetting transparency seen for the sessile water drop was also observed for the advancing water contact angle, as shown in Supplementary Fig. S1. Typical values of the contact-angle hysteresis are also provided in the Supplementary Information. Figure 2b shows the results of wetting experiments performed on Cu substrates with a varying number of graphene layers. Baseline Cu has a water contact angle of ~85.9°, which increases by ~0.7% to 86.2° for monolayer graphene. The contact angle then continues to increase very gradually to ~86.6° for 2–3-layer graphene. Beyond four graphene layers there is a relatively sharp increase to ~88.3° in the contact angle. The water contact angle finally saturates at the bulk graphite value (~90.6°) for more than six graphene layers. These results indicate that monolayer

¹Department of Mechanical, Aerospace and Nuclear Engineering, Rensselaer Polytechnic Institute, Troy, New York 12180, USA, ²Department of Materials Science and Engineering, Rensselaer Polytechnic Institute, Troy, New York 12180, USA, ³Department of Mechanical and Materials Engineering, Rice University, Houston, Texas 77005, USA. †These authors contributed equally to this work. *e-mail: pma2@rice.edu; koratn@rpi.edu.

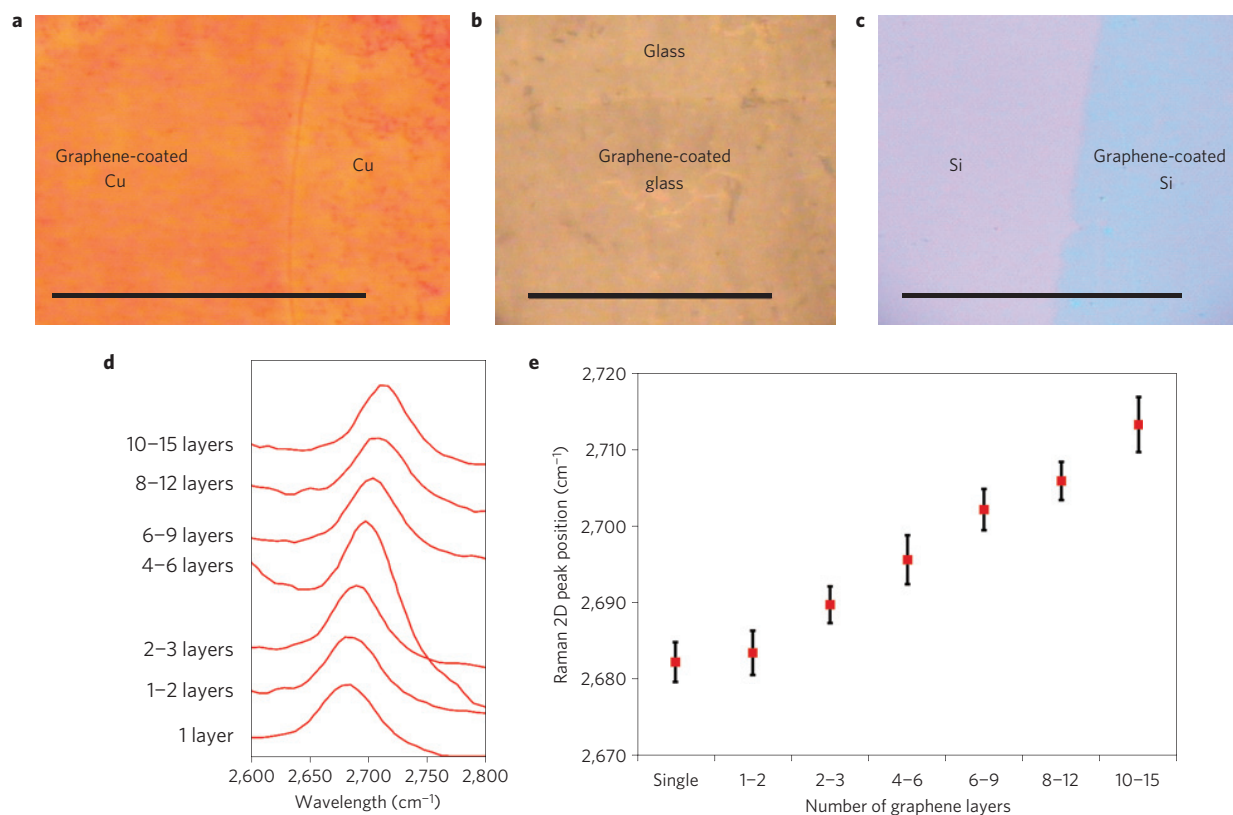


Figure 1 | Graphene film deposition. **a–c**, Large-area continuous graphene films deposited on Cu (**a**), glass (**b**) and Si (**c**) substrates. Scale bar in the optical micrographs is ~ 1 mm. **d**, Raman spectra of graphene films with varying thickness (number of layers) deposited on Cu substrates. **e**, 2D Raman peak position plotted for different numbers of graphene layers on Cu. Consistent with the literature, the 2D Raman peak shifts monotonically from $\sim 2,680$ cm^{-1} for monolayer graphene to $\sim 2,715$ cm^{-1} for 10-layer graphene.

graphene coatings offer wetting transparency to the underlying substrate. In spite of no direct contact between the water and the substrate, the water molecules seem unaffected by the presence of the graphene and experience almost the same adsorption energy to the substrate. The implication of this is that, for surfaces such as Si, Au or Cu, conformal graphene coatings may be used to modify the electrical and thermal conductivity, chemical stability and other properties of the substrate without altering in any significant way its intrinsic wettability. However, we find that the wetting transparency of graphene breaks down on surfaces such as glass, where the water contact angle is dominated by short-range chemical forces (hydrogen bonding with water). Baseline glass (with no graphene coating) cleaned by piranha etching showed a water contact angle of $\sim 20.2^\circ$ (Fig. 2c); the ideal water contact angle for clean glass is $\sim 0^\circ$, but can be as large as $\sim 30^\circ$ if the surface is allowed to relax. A monolayer graphene coating results in an abrupt increase (Fig. 2c) in contact angle to $\sim 48.1^\circ$, followed by a further increase to $\sim 94^\circ$ as the number of graphene layers on the glass is increased to ~ 6 –9 layers.

To understand the experimental observations, we have performed molecular dynamics (MD) simulations to calculate the contact angles of water droplets on the Cu surface with various numbers of graphene layers in-between. MD simulations are generally limited to nanometre-sized water droplets, which leads to non-negligible line tension force at the tri-phase junction. Therefore the predicted contact angle is usually system-size dependent and, consequently, the macroscopic contact angle must be obtained from the extrapolation of contact angles at different droplet sizes²¹. This necessitates multiple simulations with droplets of different sizes, which is computationally expensive. Here we implemented a new approach that is free of the system-size effect on the contact angle. More specifically, we have employed a thin slab water droplet

(Supplementary Fig. S2) instead of the commonly used truncated dome-shaped water droplet geometry. The advantage of this approach is that the contact line between water and the substrate is straight and thus there is no contribution of the line tension due to curvature in the Young's equation. Thus, the macroscopic contact angle can be directly calculated through fitting the x – z projection (Supplementary Fig. S2) of a nanometre-sized droplet. This new water droplet geometry yields satisfactory results when compared with a water droplet with the conventional geometry²¹ (Supplementary Table S1).

We use a series of systems, each of which contains 4,000 H_2O molecules, to obtain the contact angles of the wetting systems of $\text{H}_2\text{O}/N$ -layer-graphene/Cu (see Methods for the selection of MD parameters). The dimensions of these systems are $307.7 \text{ \AA} \times 22.2 \text{ \AA} \times 200 \text{ \AA}$. Representative snapshots for a water droplet on Cu with no graphene (seen as bulk Cu), 1-layer graphene, 3-layer graphene and 6-layer graphene (seen as graphite) in-between are shown in Fig. 3a–d respectively. The plot of the predicted contact angle versus number of graphene layers is shown in Fig. 3e. It is clear that the contact angle increases monotonically from $\sim 84.1^\circ$ to $\sim 93^\circ$ (from bulk Cu to graphite) with an increasing number of graphene layers, in agreement with the experimental observations. Above four layers of graphene, the contact angle seems to saturate at the bulk graphite value. The water contact angle for the monolayer graphene coating on Cu is $\sim 2.3\%$ greater than the baseline uncoated Cu substrate. These trends are qualitatively very similar to the experimental observations shown previously in Fig. 2b, although there are some quantitative differences; which is to be expected given the various non-ideal effects (for example, substrate roughness, wrinkling of graphene sheets and so on) that are not modelled in the simulations. Note that the cut-off for van der Waals interactions (see Methods)

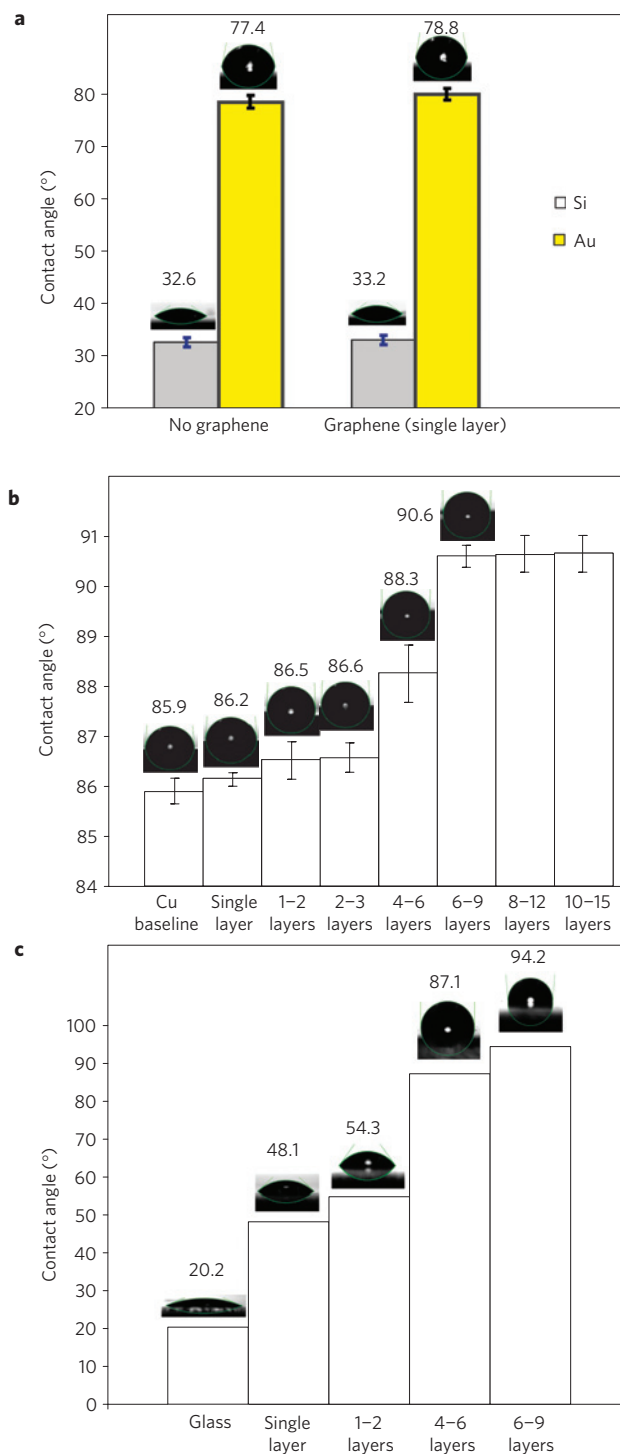


Figure 2 | Wetting transparency of graphene. **a**, Water contact angle measurements for Si and Au substrates with and without a monolayer graphene coating. The intermediate graphene layer has no significant impact on the baseline wettability of the underlying substrate. **b**, Water contact angle measurements on Cu substrates with different numbers of graphene layers. There is <0.7% change in the contact angle of the Cu substrate in the presence of monolayer graphene. Beyond four graphene layers there is a sharp decrease in the wettability, with the water contact angle finally saturating at the bulk graphite value for more than six graphene layers. **c**, Water contact-angle measurements on glass with different numbers of graphene layers. The wetting transparency effect of monolayer graphene that was seen for Cu, Au and Si is not observed on the glass substrate.

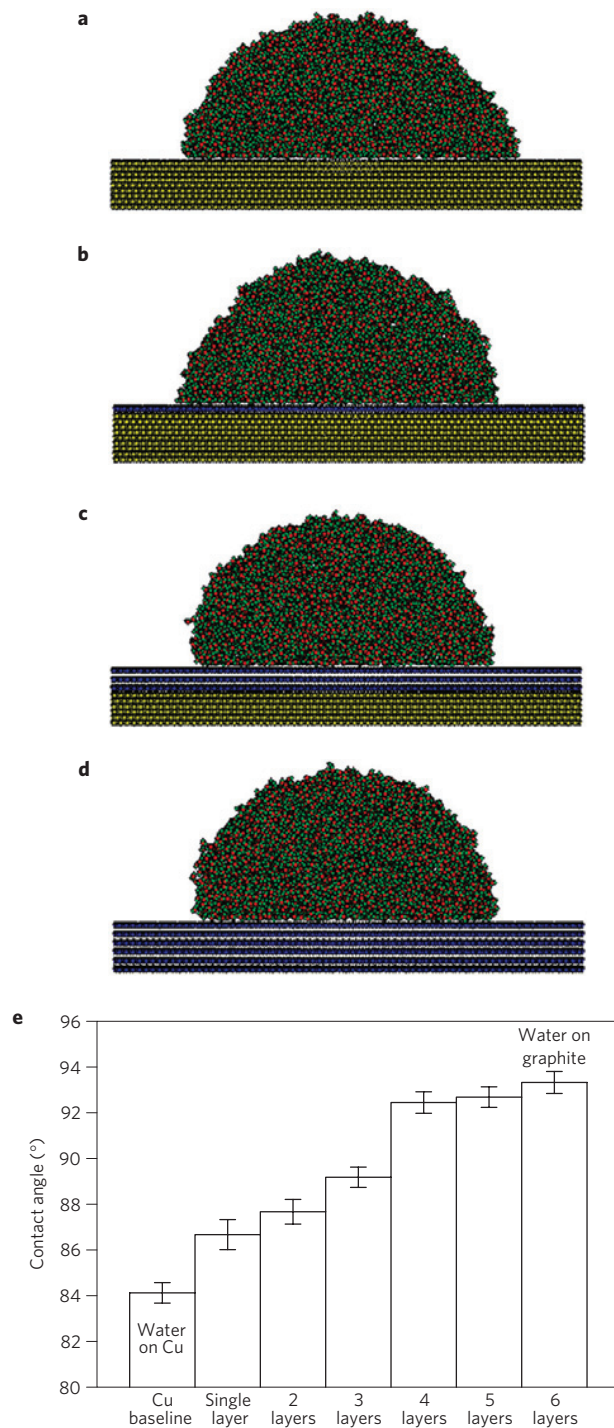


Figure 3 | Molecular dynamics simulation of water contact angle on the graphene/Cu system. **a–d**, Snapshots for 4,000 H₂O molecules on bulk Cu (**a**), monolayer graphene on a Cu substrate (**b**), 3-layer graphene on a Cu substrate (**c**) and graphite (**d**). Yellow, blue, red and green dots represent Cu, C, O and H atoms, respectively. **e**, Predicted contact-angle variation with an increasing number of graphene layers on the Cu substrate.

in our simulations was set to be 20 Å (~six layers of graphene). Therefore, the observed wetting transparency in the MD simulations is not an artefact of a small van der Waals cut-off.

The wetting transparency of graphene on Cu can be understood in terms of how the graphene layer affects the adsorption energy of water on the Cu substrate. The adsorption energy has been shown to be related to the contact angle^{22,23}. Consider a water molecule

adsorbed on the Cu substrate. It interacts with neighbouring Cu atoms within the interaction range. On the insertion of single-layer graphene between the water molecule and the Cu substrate, only the topmost layer of Cu is replaced by carbon whereas the majority of the Cu neighbours essentially remain the same (Fig. 4a). The predicted adsorption energy for Cu substrates with different numbers of graphene layers is shown in Fig. 4b. The simulations indicate that the adsorption energy of water on Cu differs by only 0.4%, with or without the monolayer graphene coating. Thus, the wetting transparency of graphene is mainly due to its two-dimensional non-close-packed thin-sheet geometry, which only slightly perturbs the adsorption energy of water molecules with the substrate. The adsorption energy decreases monotonically with an increasing number of graphene layers and saturates at \sim four layers. The contact angle of water should increase with decreasing adsorption energy (if other parameters are not changed), thus explaining the predicted contact-angle results shown in Fig. 3e.

The wetting transparency of graphene films (absent of strong short-range chemical bonding) can also be understood from continuum modelling using the effective-interface-potential approach^{24–27}. The basic idea is to consider the solid/liquid interfacial energy $W(h)$, defined as the excess free energy per unit area it takes to bring two interfaces from infinity to a certain distance h (refs 24,25). By this definition, W can be calculated from the integration of molecular pair-wise interactions across the interface²⁵. This approach has been successfully applied in the literature for understanding the dewetting of thin films^{25,27}.

The relation between the work of adhesion (which equals the negative of interfacial energy), surface free energy and contact angle (θ) can be described by the Young–Dupre equation²⁴:

$$\gamma(1 + \cos\theta) = W_{\text{ad}} = |W(h)| \quad (1)$$

The surface tension of water γ is taken^{21,25} as 0.072 J m^{-2} . To calculate the interfacial energy W , we first consider the generic half-space fluid interacting with a half-space substrate (the situation of water on Cu and water on graphite). The classic model of wetting assumes that the interaction of two surfaces is the summation of all the molecular pair-wise interactions across the interface. Thus when the van der Waals interaction is chosen in a 12–6 Lennard-Jones (LJ) form, the interfacial energy can be expressed as²⁴

$$W(h) = \frac{c}{h^8} - \frac{A}{12\pi h^2} \quad (2)$$

where h is the separation between the surfaces of interest. The Hamaker constant, A , is taken as $A_{\text{H}_2\text{O}-\text{Cu}} = 12.2 \times 10^{-20} \text{ J}$ and $A_{\text{H}_2\text{O}-\text{graphite}} = 9.08 \times 10^{-20} \text{ J}$, following the $A_{12} = (A_{11}A_{22})^{1/2}$ mixing rule^{24,28}. Here, c denotes the strength of short-range repulsion, which is taken so as to match the contact angles for water on graphite and water on Cu obtained from our experiments (85.9° for water on Cu and 90.6° for water on graphite): $c_{\text{H}_2\text{O}-\text{Cu}} = 2.52 \times 10^{-80} \text{ J m}^6$, $c_{\text{H}_2\text{O}-\text{graphite}} = 0.98 \times 10^{-80} \text{ J m}^6$. The equilibrium separations are found to be $\sim 1.77 \text{ \AA}$ and $\sim 1.59 \text{ \AA}$ for water on Cu and water on graphite, respectively.

Next, we consider the situation of water on the Cu substrate with graphene in-between. The interfacial energy for this case can be expressed as^{24,25,27}

$$W(h) = \frac{c_{\text{H}_2\text{O}-\text{graphite}}}{h^8} - \frac{c_{\text{H}_2\text{O}-\text{graphite}}}{(h+d)^8} + \frac{c_{\text{H}_2\text{O}-\text{Cu}}}{(h+d)^8} - \frac{A_{\text{H}_2\text{O}-\text{graphite}}}{12\pi h^2} + \frac{A_{\text{H}_2\text{O}-\text{graphite}}}{12\pi(h+d)^2} - \frac{A_{\text{H}_2\text{O}-\text{Cu}}}{12\pi(h+d)^2} \quad (3)$$

where h is the separation between water and the substrate and d is the thickness of the graphene film. When $d = 0$, equation (3) reduces to the correct form for the work of adhesion for water on a Cu

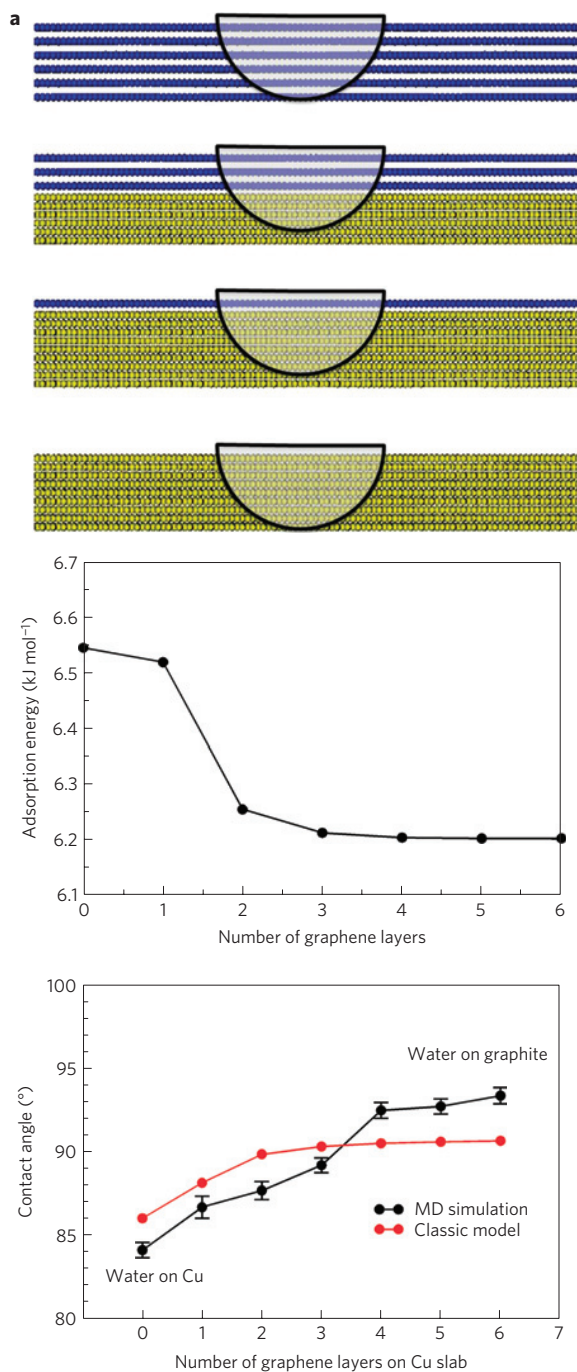


Figure 4 | Mechanism of wetting transparency. **a**, From bottom to top, illustration of the interaction range of water molecules on Cu substrates without graphene and covered with monolayer graphene, 3-layer graphene and 6-layer graphene, respectively. **b**, Predicted adsorption energy of water on Cu substrates with different numbers of graphene layers. Monolayer graphene deposition yields a minimal change in the adsorption energy. **c**, Comparison of the molecular-dynamics predictions with continuum predictions based on the classical effective-interface-potential approach.

substrate. When d approaches infinity, equation (3) reduces to the correct form for water on graphite. Figure 4c shows the comparison of contact angles for water on Cu with different numbers of layers of graphene for both the classical continuum model (equations (1) and (3)) and the MD model. The thickness of one graphene layer is assumed to be $\sim 0.34 \text{ nm}$ in the simulations. Both the classic and the MD models qualitatively reproduce the contact-angle transition

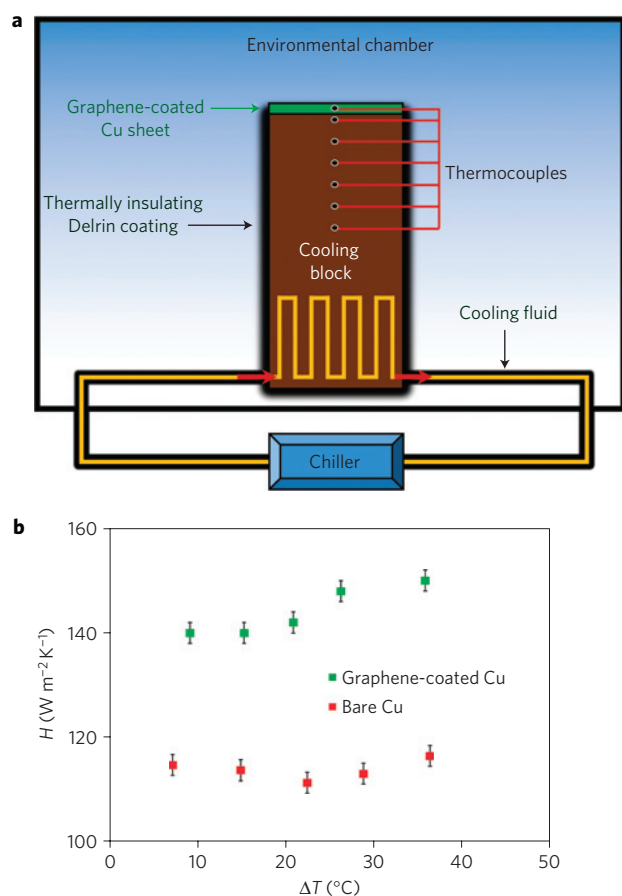


Figure 5 | Condensation heat-transfer enhancement. **a**, Test set-up showing the graphene-coated Cu sheet mounted on a thermally insulated cooling block in an environmental chamber. Cooling fluid passing through the block controls the surface temperature of the Cu sheet and the heat flux. An array of thermocouples are used to measure the temperature of the Cu sheet surface, the ambient temperature and the 1D heat flux through the cooling block. **b**, Measured condensation heat-transfer coefficient (H) for bare Cu and graphene-coated Cu at a relative humidity of $\sim 10\%$ in the chamber for different values of the difference (ΔT) between ambient temperature and the temperature of the Cu sheet.

observed in the experiments (Fig. 2b). These results indicate that the wetting transparency of graphene is attributable to its extreme thinness. The van der Waals interaction (equation (3)) is calculated by integrating the interaction of all the molecules in the fluid with all the molecules in the substrate. This integration implies additivity, which therefore results in wetting transparency of the ultrathin graphene monolayer to the relatively long-range van der Waals interactions. This analysis also explains why the wetting transparency breaks down for surfaces such as glass. In spite of its extreme thinness, the presence of graphene at the water/glass interface will disrupt the short-range chemical interactions that play a dominant role in determining the water/glass contact angle. Therefore, for surfaces where chemistry plays the dominant role, the graphene coating will not provide wetting transparency. Note that the contact-angle transition in terms of graphene layer thickness is slightly different (Fig. 4c) in the classic model and the MD model (MD being closer to experimental observations). This is probably because the continuum model considers only the film thickness and does not account for the atomic-level discreteness of the graphene film.

The ability of graphene to passivate a surface without disrupting its wetting properties could have significant practical benefit for condensation heat-transfer applications^{29,30}. Typically, Cu is the

material of choice for condensation heat transfer because of its very high thermal conductivity, but when exposed to the environment it is oxidized. The oxide layer acts as a thermal barrier, which reduces the heat transfer coefficient at Cu interfaces. Coating Cu with graphene has been shown²⁹ to prevent oxidation, which will improve the heat transfer. However, if the coating material disrupts the intrinsic wettability of Cu, then this can adversely affect condensation heat transfer. For example, if the Cu surface becomes strongly hydrophilic, condensed water forms a liquid film³⁰ on the surface that can act as an interfacial thermal barrier. Conversely, if the Cu surface becomes strongly hydrophobic, the nucleation density of condensed water drops diminishes³⁰, which also adversely affects the heat transfer. The graphene coating is unique in that it can passivate Cu oxidation without changing the intrinsic interaction of water with the Cu surface. To study the potential benefit of this, we performed condensation heat-transfer experiments on a Cu sheet (~ 40 mm in diameter) with and without monolayer-graphene deposition. As discussed in the Methods, the growth procedure of graphene on Cu reduces any native oxide present on the Cu surface. The graphene layer, once formed, prevents²⁹ any subsequent oxidation of the Cu surface. Figure 5a depicts the test set-up, which involves controlling the Cu sheet temperature below ambient temperature at a fixed humidity level in an environmental chamber. The Cu sheet was mounted on a specially designed cooling-block (insulated with Delrin to maintain 1D heat conduction). The block was cooled by flowing fluid through internal serpentine channels inside the block. A chiller was used to control the cooling-fluid temperature and thereby vary the heat flux being extracted from the sample surface. To determine the heat-transfer coefficient, H , the convective heat-transfer equation³⁰ was used:

$$\dot{Q} = H \times A \times \Delta T \quad (4)$$

where \dot{Q} , A and ΔT are the heat-transfer rate, the heat-transfer surface area and the difference between ambient temperature and the surface temperature of the Cu sheet. The heat-transfer rate (\dot{Q}) was measured using an array of thermocouples embedded inside the cooling block (Fig. 5a) together with the 1D heat-conduction equation³⁰. Figure 5b shows the measured H for bare Cu and Cu with a monolayer graphene coating at a relative humidity of $\sim 10\%$ and ambient temperature of $\sim 60^\circ\text{C}$. The graphene-coated Cu shows an approximately 30–40% increase in H over a wide range of ΔT . Enhanced condensation heat transfer is important for heat exchangers used in chip cooling, as well as for de-humidification and water-harvesting applications.

To summarize, we have shown that the extreme thinness, homogeneity and chemical inertness of graphene make it an ideal coating material from the point of view of wetting transparency. For certain systems (for example, wetting of polystyrene films on Si), relatively thick SiO layers of several nm in thickness²⁵ are able to provide transparency to polystyrene wetting on Si. In contrast, for water on solid surfaces (for example Cu), ultrathin coatings are necessary for wetting transparency. This is illustrated in Supplementary Fig. S3, where we compute the water contact-angle transition from Cu to graphite for carbon film coatings on Cu with thicknesses of 0.34 nm, 0.7 nm and 1 nm using the continuum model (equation (3)). It is clear that even ultrathin 0.7 nm or 1 nm coatings fail to provide wetting transparency. The wetting transparency effect becomes apparent only when the coating thickness is reduced to ~ 0.34 nm (that is, the thickness of graphene). Sputtered oxide or polymer films cannot rival such extreme levels of thinness. Moreover, water can form hydrogen-bonding networks with oxide layers (for example, SiO used in ref. 25), as was also observed for glass (Fig. 2c), which will disrupt the wetting transparency. In contrast, graphene's basal plane is

chemically inert and less prone to oxidation compared with other materials. Graphene is also mechanically strong and highly flexible, which makes it an ideal material for conformal coating of large-area substrates. Furthermore, graphene is conductive, providing an entirely new method to independently tune the electronic properties of a surface without changing its wetting properties.

Methods

MD simulations. For the graphene/Cu system, the interlayer spacings are 2.09 Å for Cu–Cu, 3.4 Å for graphene–graphene and 2.8 Å for graphene–Cu. Cu(111) surfaces are chosen to match the graphene lattice, which is stretched by about 4% (C–C bond distance to 1.48 Å). We use the flexible SPC model²² for water–water interactions, which consists of coulombic interactions between partial charges on O (−0.8476e) and H (+0.4238e) atoms, and an O–O LJ interaction with $\epsilon_{\text{O–O}} = 0.6502 \text{ kJ mol}^{-1}$, $\sigma_{\text{O–O}} = 3.166 \text{ Å}$ and a cutoff of 10 Å. Harmonic bond and angle constraints are used to keep the O–H distance close to 1 Å and the H–O–H angle close to 109.47°. LJ potentials are used for both C–O and Cu–O interactions. The LJ parameters are determined as $\epsilon_{\text{C–O}} = 0.3975 \text{ kJ mol}^{-1}$, $\sigma_{\text{C–O}} = 3.19 \text{ Å}$, $\epsilon_{\text{Cu–O}} = 0.7113 \text{ kJ mol}^{-1}$ and $\sigma_{\text{Cu–O}} = 3.19 \text{ Å}$ to match the experimental contact angles for water/graphite and water/Cu. A LJ cutoff of 20 Å is used for Cu–O and C–O; we intentionally selected a long cutoff (~6 times the equilibrium separation between water and graphene) to avoid an artificial wetting-angle transition due to the cutoff value for the intermolecular force field. For simplicity, the Cu and graphene layers are fixed throughout the simulation. This is acceptable, as it has been shown that the water contact angle is almost identical on either rigid or flexible substrates²¹. We start the simulation using molecules placed in a well-defined order on substrates and then let them relax in the NVT ensemble at 298 K for a sufficiently long time (~500 ps) to obtain a relaxed water droplet on the substrates. Then the sample evolves for 500 ps in the NVE ensemble for data collection. The temperature fluctuation is less than 5 K. We carried out all MD simulations using the Large-scale Atomic/Molecular Massively Parallel Simulator (LAMMPS; <http://lammps.sandia.gov/>) package.

Contact-angle measurements. The contact angle was measured using a Ramé–Hart M500 digital goniometer equipped with a dispensing needle (VICI Precision Sampling, CA, USA). First, a 1 µl water droplet was generated using the automatic dispenser of the goniometer, based on four time-controlled volume steps of 0.25 µl close to the sample surface. The sessile droplet was formed by fixing the needle and approaching the substrate parallel to the needle direction with a gentle feed rate of a few micrometres per minute. All the tests were carried out in an air environment at room temperature. The axisymmetric drop-shape analysis profile (ADSA-P) method¹³ was used to estimate the contact angle of the water droplet on the solid surface.

Substrate cleaning. To establish the wetting effect, it is essential to take extreme care to verify that the surfaces are clean. The surface of the glass was cleaned using piranha solution (60% sulphuric acid + 40% hydrogen peroxide). The glass substrates were soaked in freshly prepared piranha solution for 1 h, followed by a thorough rinse with deionized (DI) water, followed by methane, and then blown dry with dry argon. The substrates were stored in sterilized boxes to avoid any contamination. Si substrates were cut into smaller pieces and used. These substrates were first sonicated in a mixture of 1:1 acetone and isopropyl alcohol (IPA). The Si wafers were then dipped into 50% hydrofluoric solution to remove any native oxide present on the surface, rinsed with DI water, and blown dry with dry argon. As the growth procedure of graphene on Cu foils involves heating them in a hydrogen atmosphere to ~950 °C, any native oxide present on the Cu surface is reduced. Graphene is then grown on this oxide-free Cu surface by passing a carbon source. The graphene layer, once formed on the Cu, will act as a barrier to prevent any oxidation of the Cu surface, as shown in ref. 29. The PMMA on the graphene surface was removed by dissolving it using acetone, followed by an IPA rinse. Any trace PMMA remaining on the graphene film was evaporated by heating the samples to ~375 °C in a furnace with constant argon–hydrogen flow and holding the temperature for ~1 h.

Received 7 July 2011; accepted 12 December 2011; published online 22 January 2012

References

- Geim, A. K. & Novoselov, K. S. The rise of graphene. *Nature Mater.* **6**, 183–191 (2007).
- Lee, C., Wei, X., Kysar, J. W. & Hone, J. Measurement of the elastic properties and intrinsic strength of monolayer graphene. *Science* **321**, 385–388 (2008).
- Nair, R. R. *et al.* Fine structure constant defines visual transparency of graphene. *Science* **320**, 1308 (2008).
- Bonaccorso, F., Sun, Z., Hasan, T. & Ferrari, A. C. Graphene photonics and optoelectronics. *Nature Photon.* **4**, 611–620 (2010).
- Roddaro, S., Pingue, P., Piazza, V., Pellegrini, V. & Beltram, F. The optical visibility of graphene: Interference colors of ultrathin graphite on SiO₂. *Nano Lett.* **7**, 2707–2710 (2007).
- Chen, Z. P. *et al.* Three-dimensional flexible and conductive interconnected graphene networks grown by chemical vapour deposition. *Nature Mater.* **10**, 424–428 (2011).
- Li, X. *et al.* Highly conducting graphene sheets and Langmuir–Blodgett films. *Nature Nanotech.* **3**, 538–542 (2008).
- Li, X. S. *et al.* Large-area synthesis of high quality and uniform graphene films on Cu foils. *Science* **324**, 1312–1314 (2009).
- Li, X. *et al.* Transfer of large-area graphene films for high-performance transparent conductive electrodes. *Nano Lett.* **9**, 4359–4363 (2009).
- Bae, S. *et al.* Roll-to-roll production of 30-inch graphene films for transparent electrodes. *Nature Nanotech.* **5**, 574–578 (2010).
- Eda, G., Fanchini, G. & Chhowalla, M. Large-area ultrathin films of reduced graphene oxide as a transparent and flexible electronic material. *Nature Nanotech.* **3**, 270–274 (2008).
- Yavari, F. *et al.* Tunable bandgap in graphene by the controlled adsorption of water molecules. *Small* **6**, 2535–2538 (2010).
- Rafiee, J., Rafiee, M. A., Yu, Z. Z. & Koratkar, N. Superhydrophobic to superhydrophilic wetting control in graphene films. *Adv. Mater.* **22**, 2151–2154 (2010).
- Dhiman, P. *et al.* Harvesting energy from water flow over graphene. *Nano Lett.* **11**, 3123–3127 (2011).
- Sansotera, M. *et al.* Preparation and characterization of superhydrophobic conductive fluorinated carbon blacks. *Carbon* **48**, 4382–4390 (2010).
- Han, J. T., Kim, S. Y., Woo, J. S. & Lee, G. W. Transparent, conductive, and superhydrophobic films from stabilized carbon nanotube/silane sol mixture solution. *Adv. Mater.* **20**, 3724–3727 (2008).
- Zou, J. *et al.* Preparation of a superhydrophobic and conductive nanocomposite coating from a carbon-nanotube-conjugated block copolymer dispersion. *Adv. Mater.* **20**, 3337–3341 (2008).
- Darmanin, T. & Guittard, F. Molecular design of conductive polymers to modulate super-oleophobic properties. *J. Am. Chem. Soc.* **131**, 7928–7933 (2009).
- Srivastava, A. *et al.* Novel liquid precursor-based facile synthesis of large-area continuous, single, and few-layer graphene films. *Chem. Mater.* **22**, 3457–3461 (2010).
- Ferrari, A. C. *et al.* Raman spectrum of graphene and graphene layers. *Phys. Rev. Lett.* **97**, 187401 (2006).
- Werder, T., Walther, J. H., Jaffe, R. L., Halicioglu, T. & Koumoutsakos, P. On the water–carbon interaction for use in molecular dynamics simulations of graphite and carbon nanotubes. *J. Phys. Chem. B* **107**, 1345–1352 (2003).
- Zhu, S. B., Fillard, T. G. & Robinson, G. W. Flexible simple point-charge water in a self-supporting thin film. *J. Phys. Chem.* **95**, 1002–1006 (1991).
- Wang, J. Y., Betelu, S. & Law, B. M. Line tension approaching a first-order wetting transition: Experimental results from contact angle measurements. *Phys. Rev. E* **63**, 031601 (2001).
- Israelachvili, J. N. *Intermolecular and Surface Forces, 2nd edn: With Applications to Colloidal and Biological Systems* (Academic, 1992).
- Seemann, R., Herminghaus, S. & Jacobs, K. Dewetting patterns and molecular forces: A reconciliation. *Phys. Rev. Lett.* **86**, 5534–5537 (2001).
- De Gennes, P. G. Wetting: Statics and dynamics. *Rev. Mod. Phys.* **57**, 827–863 (1985).
- Seemann, R., Herminghaus, S. & Jacobs, K. Gaining control of pattern formation of dewetting liquid films. *J. Phys. Condens. Matter.* **13**, 4925–4938 (2001).
- Rajter, R. F., French, R. H., Ching, W. Y., Carter, W. C. & Chiang, Y. M. Calculating van der Waals–London dispersion spectra and Hamaker coefficients of carbon nanotubes in water from *ab initio* optical properties. *J. Appl. Phys.* **101**, 054303 (2007).
- Chen, S. *et al.* Oxidation resistance of graphene-coated Cu and Cu/Ni alloy. *ACS Nano* **5**, 1321–1327 (2011).
- Chen, X. *et al.* Nanogressed micropyrarnidal architectures for continuous dropwise condensation. *Adv. Funct. Mater.* **24**, 4617–4623 (2011).

Acknowledgements

N.A.K., P.M.A. and Y.S. thank the Advanced Energy Consortium (AEC) for funding support. N.A.K. also acknowledges funding from the USA National Science Foundation (Awards CMMI-1130215 and CBET-0853785). P.M.A. also acknowledges support from the ONR graphene MURI program. We thank Y. Peles at RPI for providing us access to the condensation heat-transfer test facility in his Lab.

Author contributions

N.A.K. and P.M.A. designed and directed the research. J.R. performed the wetting measurements and optical microscopy. H.G. fabricated the graphene samples on the various substrates. F.Y. performed the Raman characterization of the samples. A.V.T. and N.A.K. performed the condensation heat-transfer measurements. X.M. and Y.S. performed the MD simulations. X.M., Y.S. and N.A.K. carried out the continuum modelling. N.A.K., P.M.A. and Y.S. wrote the paper.

Additional information

The authors declare no competing financial interests. Supplementary information accompanies this paper on www.nature.com/naturematerials. Reprints and permissions information is available online at <http://www.nature.com/reprints>. Correspondence and requests for materials should be addressed to P.M.A. or N.A.K.